Nanoscale

RSC Publishing

PAPER

View Article Online
View Journal | View Issue

Cite this: *Nanoscale*, 2013, **5**, 2100

Percolation threshold of graphene nanosheets as conductive additives in $Li_4Ti_5O_{12}$ anodes of Li-ion batteries†

Biao Zhang, Yang Yu, Yusi Liu, Zhen-Dong Huang, Yan-bing He and Jang-Kyo Kim*

Graphene nanosheets (GNSs) have been considered as potential conductive additives for electrodes in Li-ion batteries to replace the existing carbon black (CB). Graphene has exceptionally high aspect ratio and excellent electrical conductivity, enabling the formation of extensive conductive networks at a much lower content than CB. This paper reports the beneficial effects of GNSs with a low percolation threshold on electrochemical performance of $Li_4Ti_5O_{12}$ (LTO) anodes. The experimental results show that the GNSs with a diameter of 46 μm and a thickness of 4.5 nm have a percolation threshold of 1.8 wt%. The prediction based on the interparticle distance concept gives a percolation threshold of 0.54 wt% for GNSs, which is almost an order of magnitude lower than that for CB particles. The substantially low percolation along with a high electrical conductivity of GNSs explains why the LTO anodes containing only 5 wt% GNSs deliver a much better rate capability than those with 15 wt% CB. However, a higher GNS content of 10 wt% results in re-stacking GNSs, deteriorating the diffusion of Li ions through the thickness of GNSs. The parametric study indicates that the percolation threshold of GNSs is inversely proportional to the aspect ratio of GNSs.

Received 9th October 2012
Accepted 25th December 2012

DOI: 10.1039/c2nr33099g

www.rsc.org/nanoscale

1 Introduction

Electric vehicles (EVs) have attracted tremendous attention due to the environmental issues arising from the combustion of fossil oil in the traditional vehicles powered by combustion engines. Li-ion batteries (LIBs) are considered one of the most promising power sources for future EVs due to their high energy density compared to other energy storage devices, such as lead-acid and Ni–Cd batteries.[1] Nevertheless, the energy and power densities as well as the cyclic life of LIBs need to be further improved for large-scale applications in EVs. Power density measures the capability of LIBs being charged/discharged at high current rates, where fast electron transports are accompanied by Li ion insertion/extraction. A low power density arising from the high resistance to Li ions and electron transfer is among the most critical issues limiting the widespread use of LIBs. A single major cause is the low electronic conductivity of the electrode materials. For instance, a promising new cathode material, $LiFePO_4$, has an electrical conductivity of around 10^{-7} S m^{-1} (ref. 2) whereas conductivities in the range between 10^{-11} and 10^{-6} S m^{-1} have been reported for $Li_4Ti_5O_{12}$ (LTO) depending on the preparation method.[3,4]

To increase the conductivity of electrodes, two strategies have been widely adopted: namely, (i) doping and coating of conductive phases to improve the intrinsic conductivity of active materials;[5] and (ii) incorporation of conductive additives into the electrodes to form conductive networks around the active materials.[6] Among a variety of carbon materials, carbon black (CB) is the most popular conductive additive because of its low cost, reasonably high electrical conductivity and high durability after long cyclic loading. Having a spherical shape with a typical diameter of tens of nanometers, however, makes it difficult for CB particles to form an extensive 'point to point' conductive network. As such, up to 30 wt% CB has been added in the electrodes to achieve percolation, and the percolation threshold is typically about 10–15 wt% for $LiFePO_4$ cathodes.[7] Obviously, such a high content of conductive additives sacrifices the gravimetric capacity of the electrodes. Taking advantages of their extremely high aspect ratios and electrical conductivities, nanocarbon materials, such as carbon nanotubes, carbon nanofibers and graphene nanosheets (GNSs), have been extensively studied as conductive additives, aiming at constructing conductive networks at a lower percolation threshold.[8]

Anode materials consisting of LTO particles have been widely investigated due to their excellent cyclic and safety performance although their theoretical capacities are lower than that of the traditional graphite anode. LTO has many advantages, including a negligible volume change during Li ion intercalation/extraction and the high charge/discharge plateau

Department of Mechanical Engineering, The Hong Kong University of Science and Technology, Clear Water Bay, Kowloon, Hong Kong. E-mail: mejkkim@ust.hk; Fax: +852 2358 1543; Tel: +852 2358 7207

† Electronic supplementary information (ESI) available. See DOI: 10.1039/c2nr33099g

at 1.5 V *vs.* Li/Li^+, which in turn can avoid the deposition of metallic Li on the surface of the electrode and guarantee high safety at high current rates.[9] A major drawback required to be addressed is its low electrical conductivity with an associated low power density. To improve the 'intrinsic' conductivity of LTO, two methods have been studied with varied success:[10] namely, (i) doping of metal ions, such as Li^+, Sn^{2+} and Nb^{5+} (ref. 4 and 11–13), and (ii) coating of a conductive phase, such as amorphous carbon and Ag, onto the active particle surface.[14,15] Even with these supplementary steps of material modification, conductive additives still have to be added when fabricating the electrodes for a sufficiently high 'extrinsic' conductivity.

In view of the above requirement, use of carbon materials with very high aspect ratios can significantly reduce the overall volume of conductive additives by lowering the percolation threshold. In this regard, carbon nanotubes/nanofibers are much more effective than CB.[16–18] Graphene, monolayer carbon atoms tightly packed into a 2D honeycomb lattice, possesses an excellent electrical conductivity and extremely high aspect ratio, and thus has been considered to replace the traditional conductive additive, CB.[19,20] LTO–GNS composites were prepared by growing LTO nanoparticles on the surface of GNSs, which delivered attractive electrochemical performance.[21–23] Conductive additives consisting of GNSs alone or hybrids of GNSs and CB with more than a total of 15 wt% were involved in the above studies, suspecting a detrimental effect on energy density of the electrode because GNSs/CB normally present a much lower capacity than LTO in the cut-off voltage of 1–3 V for LTO.

For efficient use of different types of conductive additives, it is necessary to evaluate their percolation thresholds so as to achieve both high gravimetric/volumetric power and energy densities of the electrodes with minimal waste of additives. Thus, the present study aims to understand the relative performance of GNSs and CB as conductive additives in terms of Li ion and electron transfer through the LTO anode material. The percolation thresholds of both LTO–GNS and LTO–CB composites are predicted based on analytical models, which are compared with experimental measurements. The effects of aspect ratio of the conductive additives on percolation threshold and the corresponding electrochemical performance of the electrodes containing them are specifically evaluated.

2 Experimental

LTO was prepared *via* a solid state reaction of Li_2CO_3 and TiO_2, which were mixed in acetone by ball milling using ZrO_2 balls for 4 h at 300 rpm h^{-1}. The slurry was dried at 60 °C overnight in the oven to obtain the LTO precursor, which was calcinated at 800 °C for 12 h in a N_2 atmosphere.[24] The product was ground and sieved using a 200 mesh screen to obtain LTO powders. GNSs were prepared using a chemical method according to our previous work.[25] 1.5 g natural graphite flakes (supplied by Asbury Graphite Mills) were mixed with a mixture of 30 ml fuming nitric acid, 45 ml sulfuric acid and 3 g potassium permanganate and kept stirring in an oil-bath at 35 °C for 24 h, and the oxidized graphite flakes were washed with 5 wt% HCl solution and de-ionized water. They were dried in a vacuum oven at 40 °C overnight and subsequently expanded at 1050 °C for 30 s in a muffle furnace. The product was then sonicated in acetone and GNSs were obtained after evaporation of acetone and drying in an oven at 60 °C overnight.

The phase structures of the powders were determined on an X-ray diffraction (XRD) system (PW1830, Philips) with CuKα radiation from 10 to 70°. Field emission transmission electron microscope (FETEM, JEOL 2010F) and scanning electron microscope (SEM, JEOL 6300F and 6700F) were used to characterize the morphologies of GNSs and electrode materials. The tap densities of the GNSs and CB powders were measured.[26]

The electrochemical tests were carried out using CR2032 coin cells. The sample slurry was prepared by mixing the active material and GNSs with a polyvinylidene fluoride (PVDF) binder after magnetic stirring in *N*-methyl-2-pyrrolidone for 4 h. The PVDF content was fixed at 10 wt% in all electrodes while the GNS content was varied from 0 to 10 wt%. Electrodes containing 15 wt% CB (Super P with a Brunauer–Emmett–Teller (BET) surface area of 62 m^2 g^{-1}, supplied by Timcal Graphite & Carbon) as a conductive additive were also prepared. The slurry was coated onto the copper foil and pellets of 12 mm in diameter were cut as electrodes. The conductivities of the electrodes and GNSs were measured using the four-point probe method (Sci. Equipment & Services). The slurry was coated on a glass substrate and GNSs were compressed into a pellet with a density of ~1.2 g cm^{-3} for conductivity measurement, and the contact points were coated with a silver paste. The cells were assembled in an Ar-filled glove box using a lithium foil as the counter electrode, 1 M $LiPF_6$ in ethyl carbonate (EC)/dimethyl carbonate (DMC) (1 : 1 by volume) as the electrolyte and a microporous polyethylene film (Celgard 2400) as the separator. The coin cells were subjected to charge/discharge cycles at different current rates between 1 and 3 V on a LAND 2001 CT battery tester. The cyclic voltammetry (CV) test was performed between 1.0 and 2.5 V at scan rates ranging from 0.2 to 5 mV s^{-1}. The electrochemical impedance spectroscopy (EIS) was carried out in the frequency range from 100 kHz to 10 mHz on an electrochemical workstation (CHI660c). GNSs prepared in this work had capacities of 52, 42, 39, 33, and 30 mA h g^{-1} when discharged at 0.5 C, 1 C, 2 C, 3 C and 4 C, respectively, at a cut-off voltage of 1–3 V (Fig. S1†). The corresponding capacities of the composite electrodes were calculated based on the weight of LTO, excluding the contributions from GNSs. Two coin cells of LTO/15 wt% CB and LTO/5 wt% GNSs were charge/discharged at 1 C for 50 cycles, followed by discharging to 1 V. They were disassembled and washed with DMC in the glove box, to examine under SEM to evaluate the change in morphology.

3 Results and discussion

The XRD pattern shown in Fig. 1a suggests that the diffraction peaks of LTO were in agreement with the standard peaks of the PDF card of no. 72-0426, confirming successful synthesis of LTO. The small peak at 27.3° corresponds to a trace of TiO_2 arising from the evaporation of the lithium source during the high temperature calcination. The LTO particles had a curved,

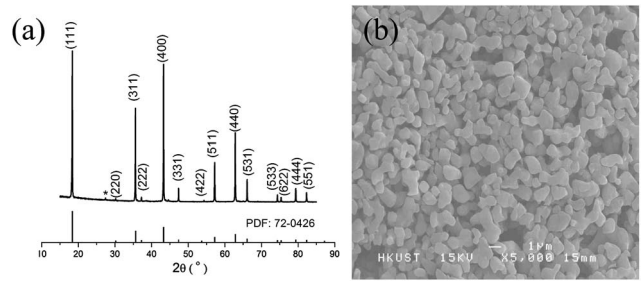

Fig. 1 (a) XRD pattern and (b) typical SEM image of LTO particles.

short rod shape with about 1–2 μm length according to the SEM image shown in Fig. 1b.

Fig. 2a and b show the morphology of CB particles that are typical of an elongated spherical shape consisting of tens of coaxial individual graphene layers with 15–30 nm in external diameter. The high degree of graphitization in CB particles gives rise to a high conductivity of about 500–3000 S m^{-1} and makes them suitable as conductive additives.[27] The GNSs shown in Fig. 2c were almost transparent and contained many wrinkles, typical of freestanding GNSs.[28] The HRTEM image shown in Fig. 2d indicates that a GNS consisted of several individual graphene layers, with an interlayer distance of 0.334 nm. The GNSs prepared using the chemical method similar to the present study typically had a thickness of about 4.5 nm and a diameter of about 46 μm on average when measured by the particle size analyzer in our previous work, which gave an aspect ratio of the magnitude of 10^4 (ref. 29). These dimensions were used to predict the percolation threshold of LTO–GNS composites in this work. The XPS analysis of GNSs indicates an O/C ratio of 0.113 by atomic concentration, indicating almost complete removal of the majority of oxygenated functional groups due to thermal reduction. The electrical conductivity measured of compressed GNS pellets was 7580 ± 700 S m^{-1}.

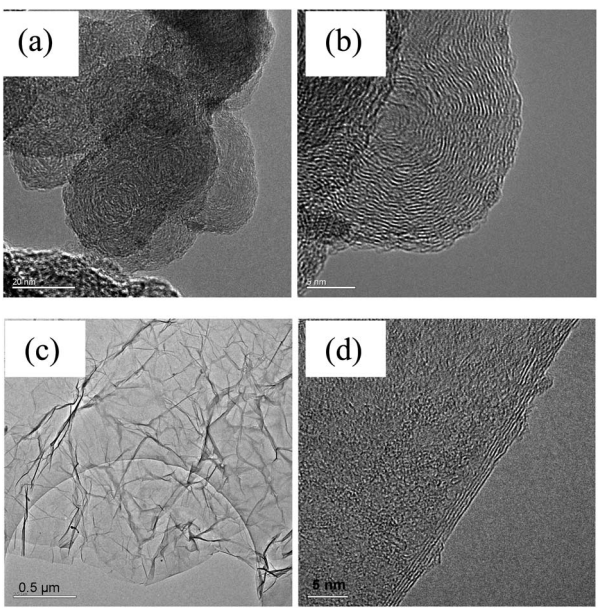

Fig. 2 TEM images of (a and b) CB particles and (c and d) GNSs.

The distribution of conductive additives in the electrodes was examined on a SEM, as shown in Fig. 3. The CB was uniformly distributed among the LTO particles (Fig. 3a). Even with a high CB content of 15 wt%, a number of LTO particles were seen exposed without full coverage by the CB particle networks, due likely to their very low aspect ratio of close to unity. The SEM micrograph of LTO electrodes with 2 wt% GNSs (Fig. 3b) showed uniform distribution of GNSs, while continuous conductive networks were assumed to be established due to the high aspect ratio of GNSs. The composite with a moderate GNS content of 5 wt% exhibited extensive conductive networks (Fig. 3c and d). Severe overlapping of GNSs was observed when the GNS content was further increased to 10 wt% (Fig. 3e and f). The GNSs with a large surface area can function as support for the LTO particles, enabling intimate contacts between the active materials and conductive additives for fast transfer of electrons during the charge/discharge process (Fig. 3d and f). However, it may be difficult for the CB particles to play a similar role as support because of the unfavorable geometry and dimensions of CB.

Fig. 4 summarizes the electrical conductivities of the LTO–GNS composite electrodes with different GNS contents. The conductivity surged by over four orders of magnitude when the GNS content was increased from 1 to 2 wt%, and only a marginal improvement was observed when the content was further increased beyond 3.5 wt%. The power law equation was employed to calculate the percolation threshold, ρ_c:

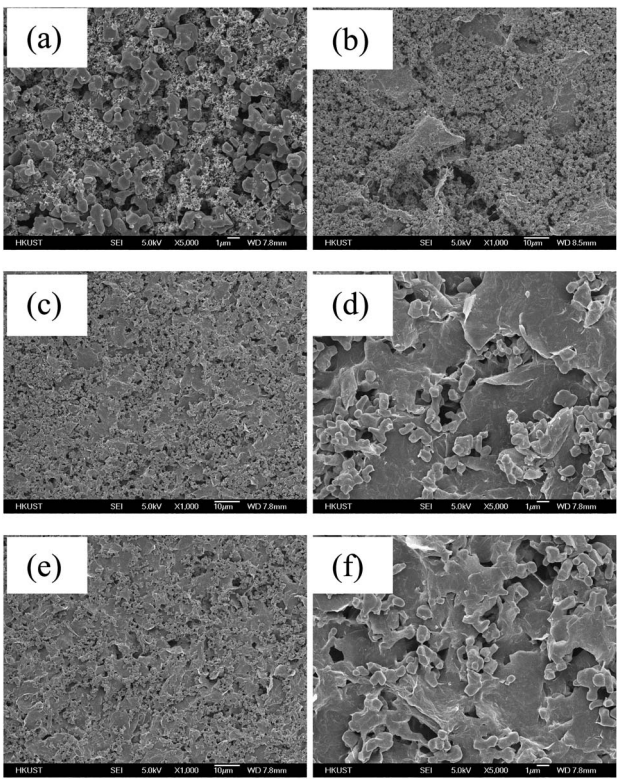

Fig. 3 SEM images of LTO electrodes with different types and contents of conductive additives: (a) 15 wt% CB; (b) 2 wt% GNSs; (c and d) 5 wt%; and (e and f) 10 wt% GNSs.

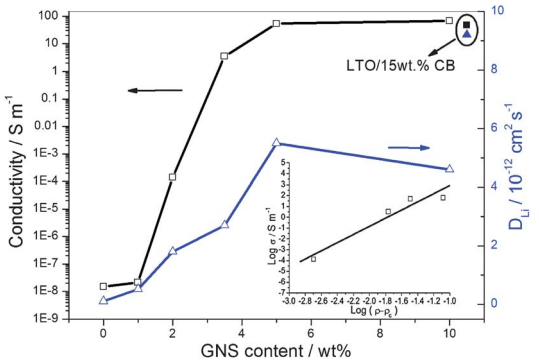

Fig. 4 Electric conductivity and Li ion transfer coefficient of LTO–GNS composite electrodes as a function of GNS content.

$$\sigma = \sigma_0(\rho - \rho_c)^n \quad (1)$$

where σ, σ_0 and ρ refer to the conductivities of the composite and filler, and the filler content, respectively; and n is the exponent.[30] The log–log plot of the conductivity data shown in the inset of Fig. 4 gave a percolation threshold of GNSs, $\rho_c = 1.8$ wt%. It should also be mentioned that the conductivity of the composite with 5 wt% GNSs was slightly higher than that of the composite with 15 wt% CB. Both the much higher aspect ratio (10^4 *vs.* ~unity) and inherent conductivity (7580 *vs.* 500–3000 S m^{-1}) of GNSs than CB were responsible for this observation.

The electrochemical performance of LTO electrodes with different conductive additives is shown in Fig. 5. The electrode with 0 and 1 wt% GNSs showed poor performance, which delivered almost zero capacity at high current rates. The capacity increased to 70 mA h g^{-1} when discharged at 0.5 C for LTO with 2 wt% GNSs arising from the improvement in conductivity (Fig. 5a). This value surged to 140 mA h g^{-1} when the GNS content was increased to 3.5 wt%, commensurate with the improvement in conductivity (Fig. 4). Nevertheless, the general performance of this electrode was marginally lower than the corresponding performance of the electrode with 15 wt% CB.

The rate capability of the electrode containing 5 wt% GNSs deserves a particular mention: it delivered increasingly higher capacities than the control electrode containing 15 wt% CB when discharged at current rates higher than 1.0 C (Fig. 5b). The capacity difference between the two electrodes increased with increasing current rate, namely by 8, 11 and 13 mA h g^{-1} when discharged at 2 C, 3 C and 4 C, respectively, again attributed to the higher conductivity of the former electrode. This finding is valid despite the fact that the Li ion diffusion coefficient was in general lower for the electrode with GNSs than that with 15 wt% CB (Fig. 4), indicating that the electrical conductivity played a more important role than the Li ion diffusion coefficient in determining the high rate capability of LTO electrodes. The low Li ion diffusion coefficient of GNSs was due probably to the inherently high resistance to Li ion diffusion through the thickness direction.[31] This phenomenon became more pronounced when a higher content was used where GNSs tended to stack on top of each other (Fig. 3f). A further increase in GNS content to 10 wt% resulted in consistent improvements in capacity at all current rates although the difference became almost negligible at a high current rate of 4 C (Fig. 5c).

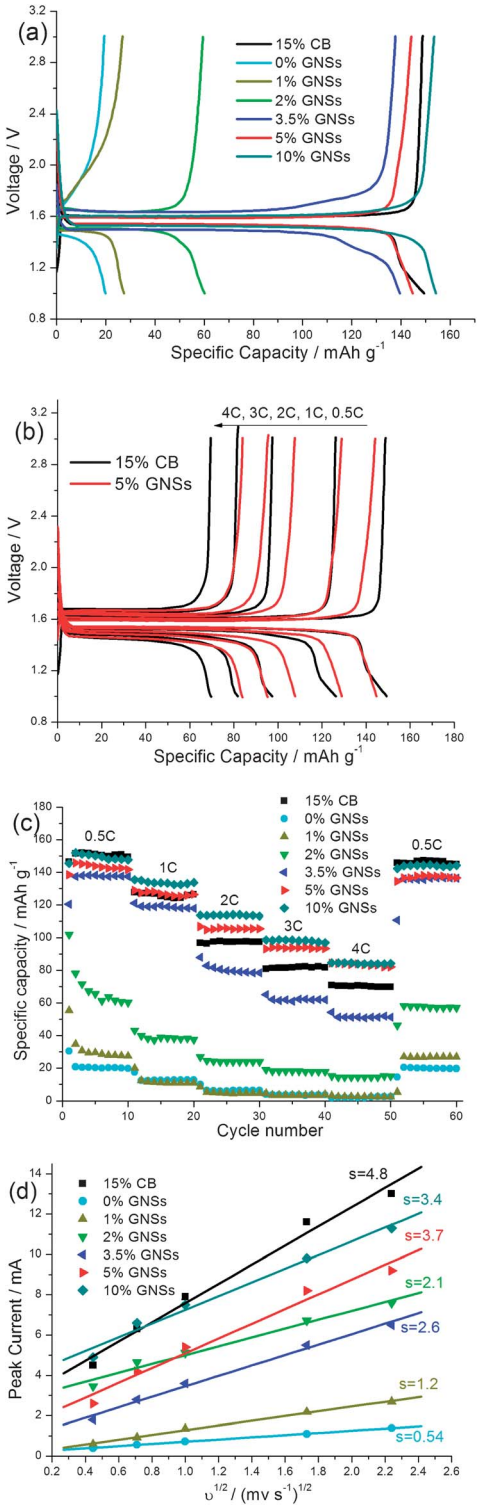

Fig. 5 Charge/discharge curves of electrodes discharged at (a) 0.5 C, (b) different current rates; (c) cyclic performance; and (d) anodic peak current plotted as a function of the square root of the scan rate in CV, where *s* represents the slope of the fitting data.

The CV tests were carried out, and the anodic peak currents obtained from the CV curves (Fig. S2†) are plotted as a function of square roots of the scan rate, as shown in Fig. 5d. The CV curves became sharp and well-defined when the GNS content increased, suggesting improvement in reaction speed. The linear relationship for all electrode materials studied indicates a diffusion-controlled reaction. The Randles–Sevcik equation was used to calculate the Li ion diffusion coefficient, D_{Li}:

$$I_p = (2.69 \times 10^5) n^{3/2} A D_{Li}^{1/2} C v^{1/2} \quad (2)$$

where I_p is the peak current; n is the number of transfer electrons; A is the surface area of the electrode; C is the concentration of reactants; and v is the scan rate. D_{Li} values obtained thereby are plotted in Fig. 4. It follows then that the LTO electrode without GNSs exhibited the lowest D_{Li} value due to the absence of conductive networks, suggesting that the GNSs served as both electron and Li ion transfer paths. An increase in GNS content from 5 to 10 wt% slightly decreased the D_{Li} value, attributed to poor diffusion of Li ions through the thickness direction when the saturated GNSs were agglomerated and stacked.[32] The SEM images in Fig. 3d and f can shed an insight into stacking of GNSs when there was a GNS content much higher than the percolation threshold. It appears that the stacked area would function as a barrier to Li ion transfer, which is responsible for the negligible capacity difference between the LTO electrodes with 5 and 10 wt% GNSs when discharged at 4 C. It should also be noticed that the GNSs have a tap density of 0.042 g cm^{-3}, which is much lower than 0.087 g cm^{-3} of CB. A high GNS content in the conductive additive would decrease the volumetric energy density of the LTO/GNS electrode. These observations indicate that an optimal GNS content should be chosen to achieve balanced properties, namely the high electronic conductivity and high Li ion diffusion coefficient, as well as the acceptable volumetric energy density. Fig. 4 also offers clear evidence that the D_{Li} value was in general higher for the electrodes containing CB than those with GNSs, a reflection of poor Li ion diffusion through the thickness of GNSs.

The SEM images of the electrodes taken after 50 cycles are shown in Fig. 6. The GNSs remained uniformly distributed and no cracks were observed in the electrodes (Fig. 6a), implying the stability of the electrodes due to negligible volume change of LTO during charge/discharge cycles. It is revealed that the LTO particles became smoothed with less angular edges and the grain boundaries of GNSs disappeared after these cycles (Fig. 6b and c), indicating the trace of reaction of LTO with the electrolyte and the deposition of a solid electrolyte interface (SEI) on the surface of electrodes (also see the high magnification images in Fig. S3†). The continuous SEI film helped avoid further reaction of LTO with the electrolyte and the generation of gases, beneficial to the cyclic performance and safety of LTO electrodes.[33,34] The EIS of the two electrodes after 50 cycles was conducted and the experimental data were fitted by the equivalent circuit shown in the inset of Fig. 6d. The SEI (R_{sei}) and charge transfer resistance (R_{ct}) values were 53.0 and 21.3 Ω for LTO/5% GNS, respectively, both of which were about

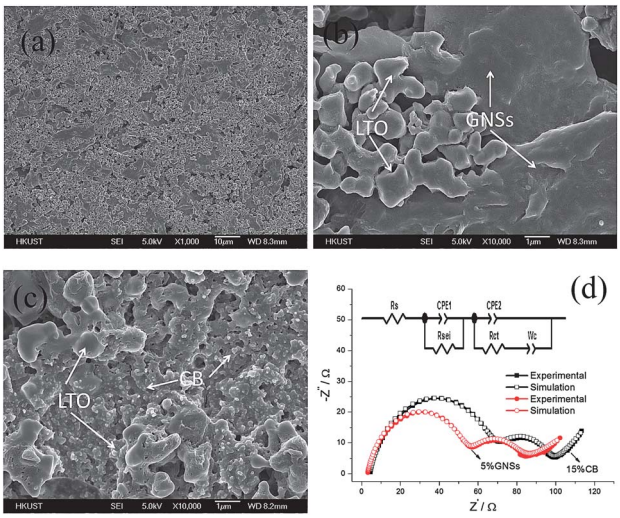

Fig. 6 SEM of electrodes: (a and b) LTO/5 wt% GNSs; (c) LTO/15 wt% CB and (d) EIS of electrodes after 50 cycles.

25% lower than 65.7 and 26.7 Ω for LTO/15% CB. The higher conductivity of the former electrode than the latter (Fig. 4) was responsible for the observation. It is necessary to limit the further growth of SEI films due to their high resistance to charge transfer. However, the influence of GNSs on the formation and thickness of SEI films is not well understood, requiring further studies.

4 Prediction of percolation threshold

An analytical model based on the average interparticle distance (IPD) concept was developed to predict the percolation threshold of conducting polymer composites containing 3D randomly distributed graphite nanosheets.[35] The same model was employed here to estimate the percolation threshold of GNSs as conductive additives in the LTO electrode. Fig. 7a illustrates the basic model where the electrode was divided into cubic elements, each of which contained a GNS. The GNSs were assumed to be uniformly distributed among the continuous medium of LTO particles and PVDF binder.

The volume fraction, V_{GNS}, required for GNSs to form continuous conductive networks when percolation occurs is given by:

$$V_{GNS} = \frac{27\pi D^2 t}{4(D + D_{Ip})^3} \quad (3)$$

where D and t are the diameter and thickness of GNSs. D_{Ip} is the interparticle distance when electron hopping happens. Similarly, the percolation threshold of conductive spherical particles, such as CB, V_{CB}, is given by:

$$V_{CB} = \frac{\pi D^3}{6(D + D_{Ip})^3} \quad (4)$$

The interparticle distance, $D_{Ip} = 10$ nm, is adopted here as the conducting criterion, according to the quantum mechanical tunneling mechanism.[36] Therefore, the predictions were

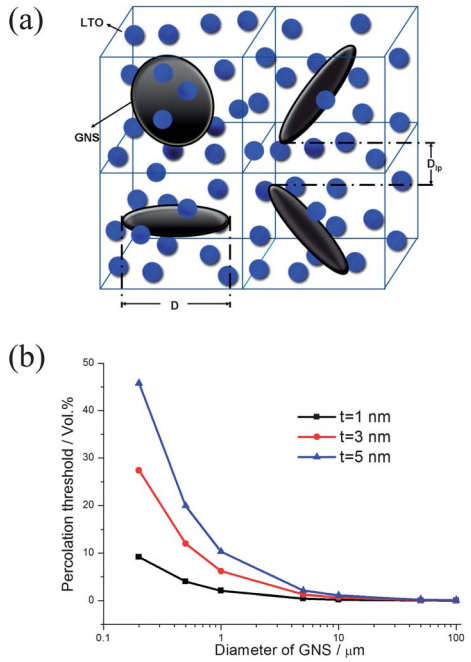

Fig. 7 (a) Three-dimensional model of a LTO–GNS composite; (b) effect of diameter of GNSs on percolation threshold.

obtained: $V_{GNS} = 0.21$ vol% for a diameter $D = 46$ μm and a thickness $t = 4.5$ nm of GNSs; and $V_{CB} = 17.3$ vol% for an average diameter $D_{CB} \approx 22.5$ nm of CB. Alternatively, the corresponding percolation threshold of GNSs in terms of weight fraction, $W_{GNS} = 0.54$ wt%, was obtained based on the simple rule of mixtures and from the known densities of the electrode constituents. The densities of LTO and GNS, $\rho_{LTO} = 0.88$ g cm^{-3} and $\rho_G = 2.26$ g cm^{-3} (ref. 29), respectively, were used in the calculation. The density of LTO particles was obtained based on the volume and weight of the electrode assuming that LTO fully occupied the volume in a cube.

It is noted that the experimental percolation threshold value (1.8 wt%) for the LTO–GNS composite electrodes was a few times higher than the predicted value (0.54 wt%). This observation is expected because the GNSs present among the LTO particles tend to be wrinkled, curved and agglomerated, effectively reducing the diameter and increasing the thickness, thus increasing the relative volume/weight of GNSs required for percolation. In addition, the electrode contains many microvoids between the LTO particles, rather than forming a continuous matrix, unlike in polymer composites, effectively increasing the measured percolation threshold value. The predicted percolation threshold of 17.3 vol% for the LTO–CB composites is considered an overestimate. This is because the CB particles studied here are not perfectly spherical, but rather of oval shape with the aspect ratio greater than one. If the change in aspect ratio is properly taken into account, the prediction may substantially drop.

A parametric study was performed to elucidate effects of dimensions of GNSs on percolation threshold, as shown in Fig. 7b. Obviously, both the diameter and thickness play an important role in determining the percolation threshold. Because $D/D_{Ip} > 100$ for the GNSs used in this study, eqn (3) can be reduced to:

$$V_G \approx \frac{21.2t}{D} \quad (5)$$

Eqn (5) signifies that the percolation threshold is inversely proportional to the aspect ratio (D/t) of GNSs. It follows then that the aspect ratio of GNSs for use as conductive additives should be maintained as large as possible. Synthesis of ultra-large, monolayer GNSs with size up to a few hundred micrometers has been reported.[37,38] In addition, destructive processes, such as ultra-sonication and mechanical vibration, should be minimized during the fabrication of composite electrodes to avoid damage to GNSs and thus to preserve their large aspect ratios for a low percolation content.

5 Conclusion

In an effort to achieve both high gravimetric/volumetric power and energy densities of electrodes with minimal waste of conductive additives, the conducting behavior and percolation threshold of GNSs and CB were studied. The relative performance of GNSs and CB in terms of Li ion and electron transfer through the LTO anode material was evaluated along with the corresponding electrochemical performance of the electrodes. The following can be highlighted from the analytical and experimental studies.

(i) The percolation threshold of GNSs with an aspect ratio of over 10^4 was measured to be 1.8 wt% in LTO electrodes. According to the interparticle distance concept, the predicted percolation threshold was 0.54 wt% for GNSs, which is almost an order of magnitude lower than that for CB particles, confirming the tremendous benefits of using GNSs as conductive additives in electrodes.

(ii) An optimal GNS content of 5 wt% in LTO electrodes delivered much improved rate capability compared to that containing 15 wt% CB, attributed to both the high aspect ratio and conductivity of GNSs. A higher GNS content of 10 wt% did not further improve the high rate capability of the anode due to the counterbalance between the marginal increase in conductivity and the large reduction in Li ion diffusion coefficient. The high GNS content meant re-stacking of GNSs, which in turn deteriorated the diffusion of Li ions through the thickness direction.

(iii) The analytical model indicates that the percolation threshold is inversely proportional to the aspect ratio of GNSs. The percolation threshold can be effectively reduced by producing monolayer, ultra-large GNSs with minimal destructive processes, such as ultra-sonication and mechanical vibration during the synthesis process.

Acknowledgements

This project was supported by the Research Grants Council of the Hong Kong SAR (Project codes: 613811 and 613612). The authors also appreciate the technical assistance from the Materials Characterization and Preparation Facilities (MCPF) of

HKUST. BZ was supported partly by the Postgraduate Scholarship through the Nanoscience and Technology Program at HKUST.

References

1 J. Tarascon and M. Armand, *Nature*, 2001, **414**, 359–367.
2 J. Ma, B. H. Li, H. D. Du, C. J. Xu and F. Y. Kang, *J. Solid State Electrochem.*, 2012, **16**, 1–8.
3 C. H. Chen, J. T. Vaughey, A. N. Jansen, D. W. Dees, A. J. Kahaian, T. Goacher and M. M. Thackeray, *J. Electrochem. Soc.*, 2001, **148**, A102–A104.
4 H. Ge, N. Li, D. Y. Li, C. S. Dai and D. L. Wang, *Electrochem. Commun.*, 2008, **10**, 1031–1034.
5 J. Wang and X. Sun, *Energy Environ. Sci.*, 2012, **5**, 5163–5185.
6 X. L. Li, F. Y. Kang, X. Bai and W. C. Shen, *Electrochem. Commun.*, 2007, **9**, 663–666.
7 A. Awarke, S. Lauer, S. Pischinger and M. Wittler, *J. Power Sources*, 2011, **196**, 405–411.
8 X. M. Liu, Z. D. Huang, S. W. Oh, B. Zhang, P. C. Ma, M. M. F. Yuen and J. K. Kim, *Compos. Sci. Technol.*, 2012, **72**, 121–144.
9 T. Ohzuku, A. Ueda and N. Yamamoto, *J. Electrochem. Soc.*, 1995, **142**, 1431–1435.
10 T. F. Yi, L. J. Jiang, J. Shu, C. B. Yue, R. S. Zhu and H. B. Qiao, *J. Phys. Chem. Solids*, 2010, **71**, 1236–1242.
11 B. Zhang, Z. D. Huang, S. W. Oh and J. K. Kim, *J. Power Sources*, 2011, **196**, 10692–10697.
12 T. F. Yi, Y. Xie, J. Shu, Z. H. Wang, C. B. Yue, R. S. Zhu and H. B. Qiao, *J. Electrochem. Soc.*, 2011, **158**, A266–A274.
13 H. S. Li, L. F. Shen, X. G. Zhang, P. Nie, L. Chen and K. Xu, *J. Electrochem. Soc.*, 2012, **159**, A426–A430.
14 E. Kang, Y. S. Jung, G. Kim, J. Chun, U. Wiesner, A. C. Dillon, J. K. Kim and J. Lee, *Adv. Funct. Mater.*, 2011, **21**, 4349–4357.
15 Z. Liu, N. Zhang, Z. Wang and K. Sun, *J. Power Sources*, 2012, **205**, 479–482.
16 B. Zhang, Y. S. Liu, Z. D. Huang, S. W. Oh, Y. Yu, Y. W. Mai and J. K. Kim, *J. Mater. Chem.*, 2012, **22**, 12133–12140.
17 X. L. Li, F. Y. Kang and W. C. Shen, *Carbon*, 2006, **44**, 1334–1336.
18 L. F. Shen, C. Z. Yuan, H. J. Luo, X. G. Zhang, K. Xu and F. Zhang, *J. Mater. Chem.*, 2011, **21**, 761–767.
19 L. Grande, V. T. Chundi, D. Wei, C. Bower, P. Andrew and T. Ryhänen, *Particuology*, 2012, **10**, 1–8.
20 F. Y. Su, Y. B. He, B. H. Li, X. C. Chen, C. H. You, W. Wei, W. Lv, Q. H. Yang and F. Y. Kang, *Nano Energy*, 2012, **1**, 429–439.
21 L. F. Shen, C. Z. Yuan, H. J. Luo, X. G. Zhang, S. D. Yang and X. J. Lu, *Nanoscale*, 2011, **3**, 572–574.
22 H. Kim, S. Bak and K. Kim, *Electrochem. Commun.*, 2010, **12**, 1768–1771.
23 Y. Shi, L. Wen, F. Li and H. Cheng, *J. Power Sources*, 2011, **196**, 8610–8617.
24 B. Zhang, H. Du, B. Li and F. Kang, *Electrochem. Solid-State Lett.*, 2010, **13**, A36–A38.
25 Y. Geng, S. J. Wang and J. K. Kim, *J. Colloid Interface Sci.*, 2009, **336**, 592–598.
26 J. Gao, C. Y. Jiang, J. R. Ying and C. R. Wan, *J. Power Sources*, 2006, **155**, 364–367.
27 V. Palomares, A. Goni, I. Gil de Muro, I. de Meatza, M. Bengoechea, I. Cantero and T. Rojo, *J. Power Sources*, 2010, **195**, 7661–7668.
28 Q. B. Zheng, W. H. Ip, X. Y. Lin, N. Yousefi, K. K. Yeung, Z. G. Li and J. K. Kim, *ACS Nano*, 2011, **5**, 6039–6051.
29 J. Li, M. L. Sham, J. K. Kim and G. Marom, *Compos. Sci. Technol.*, 2007, **67**, 296–305.
30 N. Yousefi, M. M. Gudarzi, Q. B. Zheng, S. H. Aboutalebi, F. Sharif and J. K. Kim, *J. Mater. Chem.*, 2012, **22**, 12709–12717.
31 X. Zhao, C. M. Hayner, M. C. Kung and H. H. Kung, *ACS Nano*, 2011, **5**, 8739–8749.
32 X. Zhao, C. M. Hayner, M. C. Kung and H. H. Kung, *Adv. Energy Mater.*, 2011, **1**, 1079–1084.
33 Y. B. He, B. Li, M. Liu, C. Zhang, W. Lv, C. Yang, J. Li, H. Du, B. Zhang, Q. H. Yang, J. K. Kim and F. Y. Kang, *Sci. Rep*, 2012, **2**, 913, DOI: 10.1038/srep00913.
34 M. Kitta, T. Akita, Y. Maeda and M. Kohyama, *Langmuir*, 2012, **28**, 12384–12392.
35 J. Li and J. K. Kim, *Compos. Sci. Technol.*, 2007, **67**, 2114–2120.
36 G. R. Fiuschau, S. Yoshikawa and R. E. Newnham, *J. Appl. Phys.*, 1992, **72**, 953–959.
37 X. Li, C. W. Magnuson, A. Venugopal, R. M. Tromp, J. B. Hannon, E. M. Vogel, L. Colombo and R. S. Ruoff, *J. Am. Chem. Soc.*, 2011, **133**, 2816–2819.
38 S. H. Aboutalebi, M. M. Gudarzi, Q. B. Zheng and J. K. Kim, *Adv. Funct. Mater.*, 2011, **21**, 2978–2988.

